Second Revised Version 15 March 2009

Oxygen Exchange in Uranyl Hydroxide Via Two "Non-Classical" Ions.

Michael Bühl,[a] **Georg Schreckenbach**[b]

School of Chemistry, University of St. Andrews, North Haugh, St. Andrews, Fife KY16 9ST, UK
Department of Chemistry, University of Manitoba, Winnipeg, Manitoba, Canada, R3T 2N2

Abstract

A recently proposed pathway for scrambling of axial (uranyl) and equatorial O atoms in $[UO_2(OH)_4]^{2-}$ (**1**) is refined using Car-Parrinello molecular dynamics (CPMD) simulations in an explicit solvent (water) and with model counterions (NH_4^+). According to constrained CPMD/BLYP simulations and thermodynamic integration, **1** can be deprotonated to $[UO_3(OH)_3]^{3-}$ with a T-shaped UO_3 group (ΔA = 7.1 kcal/mol), which in turn can undergo a solvent-assisted proton transfer via a *cis*-$[UO_2(OH)_4]^{2-}\cdot OH^-$ complex and a total overall barrier of $\Delta A^{\ddagger}$ = 12.5 kcal/mol. According to computed relative energies of *trans*- and *cis*-$[UO_2(OH)_4]^{2-}$ in the gas phase and in a polarizable continuum, "pure" functionals such as BLYP underestimate this overall barrier somewhat, and estimates of $\Delta A^{\ddagger} \approx$ 16 kcal/mol and 17 kcal/mol are obtained at the B3LYP and CCSD(T) levels, respectively, in excellent agreement with experiment.

[a]University of St. Andrews; Fax: (+44)(0)1334 463808, E-mail: buehl@st-andrews.ac.uk
[b]University of Manitoba

1. Introduction

Uranium chemistry is blossoming not only because of its obvious relevance to the nuclear energy platform, but also because new and exciting insights into the chemical bond can be gained at this outpost of the Periodic Table.[1] The rich chemistry of pentavalent uranium compounds[2] or the unexpected Lewis basicity of uranyl(VI) moieties[3] are just a few recent examples. Clearly, the view of the linear UO_2^{2+} unit as inert spectator that just assembles ligands in its equatorial plane is in need of refinement. Evidence for active participation of this moiety in chemical reactions also in an aqueous environment has been provided in highly alkaline solutions with a large excess of NMe_4OH.[4] Clark and coworkers have reported isotope-labelling NMR and Raman studies that have pointed to a remarkably facile oxo-ligand exchange between equatorial and axial positions, with a free energy barrier of only $\Delta G^{\ddagger} = 15.2$ kcal/mol ($\Delta H^{\ddagger} = 9.8 \pm 0.7$ kcal/mol) for this process at room temperature. Because the hydroxy complex **1** is predominant under these conditions,[5] it is reasonable to assume that this complex is involved in the scrambling process (boxed reaction in Scheme 1).

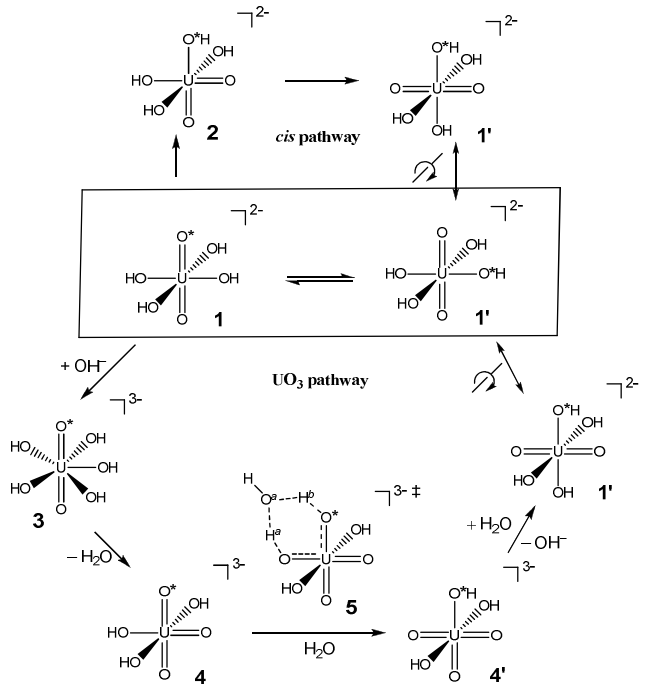

Scheme 1. Oxygen exchange in uranyl hydroxide (in box) with two possible mechanistic pathways above and below. Identical complexes in different orientation are connected by rotation signs.

More recently, this interpretation has been challenged. According to a study by Szabo and Grenthe in 2007, in pure solutions of **1** no such "yl-exchange" can be detected at all.[6] They provided evidence for a binuclear exchange mechanism under acidic conditions, i.e. involving cationic species with a $[(UO_2)_2(OH)_2]^{2+}$ core, and suggested that in the experiments of Clark et al., this yl-exchange may have to some extent already taken place during formation of the test solutions and that the actual exchange

process monitored by dynamic NMR would rather correspond to one between **1** and a pentakis(hydroxy) species **3** (which has been reported to be in equilibrium with **1**.[4] As a result of an experimental oversight, however, Szabo and Grenthe have now revised this interpretation[7] (see below).

Spurred by the initial report from the Clark group, Schreckenbach and coworkers have studied possible mechanisms for yl-exchange in **1** by quantum-chemical computations at suitable levels of density-functional theory (DFT).[8,9] A possible mechanism could involve a *cis*-uranyl species **2** (upper path in Scheme 1). In keeping with the elusiveness of such species, **2** has been computed to be quite high in energy (18-19 kcal/mol above **1**).[8] Because an additional activation energy for proton transfer would be needed, this path would seem unlikely. Based on results at the PBE-ZORA/COSMO level, Shamov and Schreckenbach have recently proposed an alternative route via a tris(oxo) species **4** as key intermediate.[9] Accessible through water elimination from the pentakis(hydroxy) species **3** (which, in turn, has been reported to be in equilibrium with **1**)[4] , **4** can undergo a facile, solvent-assisted proton shuttling process via transition state **5**. This process appeared in fact so facile that water elimination from **3** emerged as rate-limiting step in these computations, with a barrier in good apparent accord with the data reported by Clark et al. **4** would be an intriguing derivative of molecular UO_3, which is only known in the gas phase.[10]

These computational data seemed to be in conflict with Szabo and Grenthe's results. If, as suggested by theory, there would be such a viable yl-exchange path for **1**, why should it not be observed in this system? Before they can be used to assess experiments, quantum-chemical computations must be scrutinized for their accuracy. For actinides[11] this requires the adequate treatment of three, largely independent methodological issues: (i) the model chemistry (defined by the one-particle basis set and the theoretical level of treating the many-body interactions); (ii) relativity; and (iii) solvation.[12] As for issues (i) and (ii), hybrid DFT and small-core relativistic effective core potentials (ECPs) or all-electron relativistic treatments such as the zeroth-order regular approximation (ZORA) have proven fairly robust in describing the thermochemistry of actinides.[13] Because **1** is a closed-shell f^0 system, spin-orbit coupling can safely be neglected. Based on these considerations, there is little reason to doubt the accuracy, at least in a qualitative sense, of Shamov and Schreckenbach's results for **1**. Point (iii), solvation, is more critical, as the species involved are highly charged (e.g., **4** is a trivalent ion) and the experiments refer to aqueous solution with its high polarity and hydrogen bonding capability. Especially the latter interactions are difficult to describe with a simple polarizable continuum model (PCM) such as the COSMO approach as used by Shamov and Schreckenbach. In fact, static PCM calculations can perform remarkably poorly already for divalent ions, e.g. for the acidity constant[14] or the halide binding energies[15] of uranyl hydrate, $[UO_2(H_2O)_5]^{2+}$. In these[15,16] and other cases[17] involving uranyl(VI) species, DFT-based Car-Parrinello molecular dynamics (CPMD) simulations using the BLYP functional and pointwise

thermodynamic integration (PTI) have performed very well, reproducing experimental free energies and activation barriers with an accuracy of ca. ±2.5 kcal/mol for a number of complexes.[15-17] We now apply this methodology to the intriguing yl-exchange mechanism in **1**, striving to refine the previous static PCM calculations. As it turns out, dynamics and explicit solvation affect some mechanistic details along the computed reaction path, but not the overall barrier. This renewed support of Clark et al.'s initial observation has led Szabo and Grenthe to reinvestigate and revise their own NMR evidence,[7] resulting in a nice agreement between experimental and calculated activation energies.

2. Computational Details

The same methods and basis sets as in our previous studies of uranyl fluorides and hydroxides were employed.[15] Car-Parrinello molecular dynamics (CPMD)[18] simulations were performed using the BLYP functional[19] and norm-conserving pseudopotentials that had been generated according to the Troullier and Martins procedure[20] and transformed into the Kleinman-Bylander form.[21] For uranium, the semicore (or small-core) pseudopotential was employed that had been generated and validated in reference 22. Periodic boundary conditions were imposed using cubic supercells with a lattice contant of 13 Å. Kohn-Sham orbitals were expanded in plane waves at the Γ-point up to a kinetic energy cutoff of 80 Ry. Simulations were performed in the NVT ensemble using a single Nosé-Hoover thermostat set to 320 K (frequency 1800 cm^{-1}), a fictitious electronic mass of 600 a.u., and a time step of 0.121 fs. The somewhat higher temperature was chosen to increase solvent mobility and improve the sampling. The boxes contained 55 extra water molecules (or 54 H_2O and one OH^-) and three NH_4^+ ions, affording a density of ca. 1.0. In order to maintain the time step, hydrogen was substituted with deuterium. Long-range electrostatic interactions were treated with the Ewald method. No electrostatic decoupling between replicated cells was included, as it had been shown that no noticeable errors are introduced by this procedure for divalent ions,[23] and no artifacts were apparent even for trivalent ones.[24] The BLYP functional was chosen because it performs better than most other standard GGAs for describing the properties of liquid water.[25]

Constrained CPMD simulations were performed along predefined reaction coordinates ξ (bond distances r or differences in bond distances Δr), in order to evaluate the change in the Helmholtz free energy by pointwise thermodynamic integration[26] of the mean constraint force $\langle f \rangle$ along these coordinates via

$$\Delta A_{a \to b} = -\int_a^b \langle f(\xi) \rangle \mathrm{d}\xi \qquad (1).$$

At each point, the system was propagated until $\langle f \rangle$ was sufficiently converged (usually within 1.5 - 2 ps after 0.5 ps of equilibration), similar to the degree of convergence documented in Figure S1 of the supporting information for reference 22. Each new point was continued from the final, equilibrated configuration of the previous one, using 2000 steps of continuous slow growth to increase (or decrease) the

constrained coordinate. While some hysteresis cannot be excluded that way, its extent appears to be limited, as judged from the close correspondence of much of the closely related "forward" and "reverse" paths of the proton-shuttling process (see Table S1 in the Supporting Information). In order to avoid deprotonation of the NH_4^+ ions, all 12 NH bond distances were kept fixed at 1.05 Å, the value adopted in ref. [27]. Because the simulations were performed at constant volume, Helmholtz rather than Gibbs free energies are obtained, but in condensed phase the difference between both should be very small. No further dissection of the free energies into enthalpic and entropic contributions (which would require, in principle, simulations at different temperatures) was attempted. These computations were performed with the CPMD program.[28]

The starting structure for the deprotonation path (Figure 1 below) was generated from the last point of the constrained OH^- dissociation path from **3** in ref. 27. The simulation with a constrained U-O distance of 4.3 Å (i.e. the endpoint of the corresponding profile in Figure 2 of ref. 27) was continued without this constraint for 3 ps. The arrangement corresponding to **1**·OH^- with the inner-sphere OH ligand donating a H-bond to the outer-sphere hydroxide remained stable during this time, and the OH distance eventually used as reaction coordinate fluctuated around r = 1.00(3) Å. Beyond the endpoint of this path, i.e. at r > 1.6 Å, the constraint force remains essentially zero. When the last point was continued for 2 ps without this constraint, the corresponding O···H distance fluctuated around 1.85(25) Å.

For the proton shuttle pathway (Figure 3 below), two continuous paths were constructed from the same starting point at Δr = 0 (corresponding to **5**, or rather, **2**·OH^-). The initial structure was generated from the last point of the deprotonation pathway (Figure 1) by manually moving a water molecule from the first hydration sphere into an appropriate position and adjusting the OH distances accordingly. After 2 ps of simulation with Δr = 0, this constraint was gradually incremented in steps of +0.2 Å and –0.2 Å until final values of Δr = ±1.0 Å were reached. The "forward" path was further extended up to Δr = +1.1 Å.

Static, non-periodic geometry optimizations for pristine **1** and **2** were performed in the gas phase using BLYP and B3LYP[29,19b] functionals, the small-core Stuttgart-Dresden relativistic ECP together with its valence basis set[30] (from which the most diffuse s-,p-,d-, and f-functions were omitted each, affording a [7s6p5d3f] contraction), and 6-311+G(d,p) basis[31] on all other elements. Geometries were fully optimized in the given symmetries and conformations, and the minimum character was confirmed in each case by computation of the harmonic vibrational frequencies. Single point energies were evaluated for the gas-phase geometries using the same methods and basis sets, together with the PCM approach of Tomasi and coworkers[32] (employing the united-atom UFF radii and the parameters of water). Additional single-point

energy calculations have been performed in the gas-phase at various wavefunction-based levels up to CCSD(T), employing the B3LYP/SDD/6-311+G(d,p) geometries and SDD(g)/aug-cc-pVTZ basis, i.e. the abovementioned SDD ECP and valence basis, augmented with a set of g-functions (exponent 0.5),[13] and aug-cc-pVTZ basis[33] for O and H. More DFT single points have been computed with the same basis set and geometries, including PBE[34] and the recent Minnesota functionals M06-L,[35] M06,[36] and M06-2X.[36] These calculations were performed with the Gaussian[37] and Molpro[38] suite of programs.

3. Results

Initial attempts to simulate the pristine tris-anions **3** or **4** in a periodic water box were thwarted by their tendency to deprotonate a water molecule from the first hydration sphere, rapidly affording complex **1**. In a recent CPMD study on counterion effects we had found that aqueous **3** remained metastable for a few picoseconds when three rigid NH_4^+ ions were added as counterions.[27] These ions are not meant to represent the more hydrophobic NMe_4^+ ions used in the studies of uranyl hydroxide, but are viable models for discrete ions in the vicinity of the metal complex.[39] This setup also allowed the application of the CPMD-PTI approach, according to which **3** turned out to be higher in free energy than **1** + OH^- by ΔA = 4.4 kcal/mol. Thus, we used the same setup including NH_4^+ counterions to model the yl-exchange pathway in **1**.

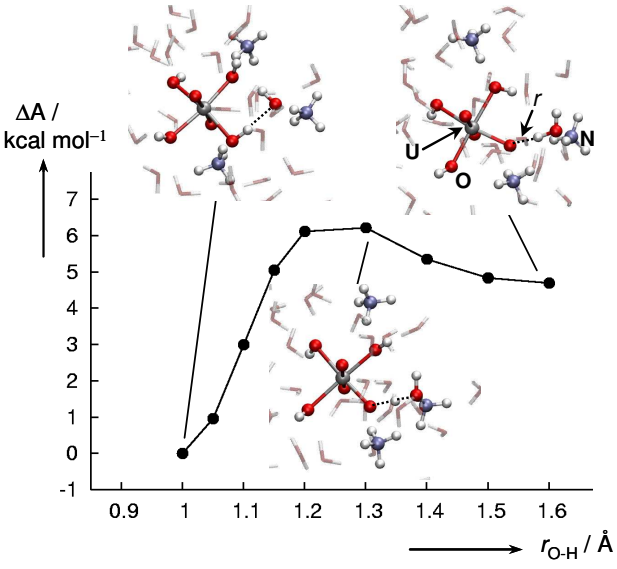

Figure 1. CPMD/BLYP simulated free-energy profile from **1**·OH^- (left) to **4** (right) at 320 K, using a UO···H distance as reaction coordinate. Representative snapshots from selected points are included.

3.1 Deprotonation Step

Rather than modeling water elimination from **3** (as had been done by Shamov and Schreckenbach and is sketched in Scheme 1),[9] we decided to attain the tris(oxo) intermediate **4** in a more direct way, by deprotonation of **1**.[40] To this end, we prepared a well-equilibrated **1**·OH^- configuration including three NH_4^+ counterions (see Computational Details). During 3 ps a configuration was maintained, in which the "free" hydroxide ion accepts an H-bond from one of the metal-bound OH^- ligands (dotted line in the top left snapshot in Figure 1). Subsequently, the O-H distance of this ligand was fixed and used as reaction coordinate by successive incremental increase from r = 1.0 Å, affording the free-energy profile displayed in Figure 1. Passing a barrier at r = 1.3 Å ($\Delta A^{\ddagger}$ = 6.2 kcal/mol), the free energy levels off at r = 1.6 Å, at a value of ΔA = 4.7±0.6 kcal/mol.

What is missing in order to assess the stability of **4** is the "penalty" for forming the ion pair **1**·OH^- from the separated constituents. Following simple electrostatic arguments, formation of such an outer-sphere complex of two ions with charges of −2 and −1 is estimated to be endergonic by ΔG = +2.4 kcal/mol.[41] When this number is added to our simulated ΔA value, **4** is predicted to be less stable than **1** + OH^- by 7.1 kcal/mol. The tris(oxo) species **4** is thus indicated to be a very strong base in water. This finding is consistent with EXAFS experiments for alkaline solutions of **1**, that were interpreted solely in terms of an equilibrium between **1** and **3**, and found no evidence for significant population of **4**.[5]

Significantly, **4** is indicated to have a small, but noticeable barrier for the reverse reaction, deprotonation of water (1.5 kcal/mol on the path from right to left in Figure 1), and should thus be metastable on the picosecond timescale. We therefore set out to construct a path describing the solvent-assisted proton-shuttle process for **4** that completes the oxygen exchange (bottom of Scheme 1) and that is central to Shamov and Schreckenbach's proposed mechanism.

3.2 Proton-Shuttle Pathway

For this purpose, we used the difference Δr between the breaking and forming O···H bonds at the solvent relay as reaction coordinate [i.e. $r(O^a\text{-}H^a) - r(O^a\text{-}H^b)$ in structure **5** in Scheme 1]. Starting at Δr = 0 (corresponding to **5**), both forward and backward paths leading to the two variants of **4** were followed up to Δr = ±1.0 Å in steps of ±0.2 Å. In addition, the forward path was continued up to Δr = +1.1 Å (the mean value from a 1 ps simulation without that constraint and approximately zero mean force). Retracing the "reverse" path from Δr = −1.0 Å to zero and continuing all the way to $\Delta r \approx$ +1.0 Å thus describes a continuous path for the proton shuttle converting the tris(oxo) species **4** into its yl-scrambled isomer. As illustrated in Figure 2, a plot of salient OH distances along this path, this process is initiated by a proton

transfer from the water molecule (H^b in Figure 2, see blue and green lines at $t \approx -4$ ps), affording **2**·OH^- (see also section 3 below). Stable over a significant part of the path, the latter eventually collapses to the rearranged product by way of a second proton transfer to the hydroxide (H^a, see orange and black lines at $t \approx 5$ ps).

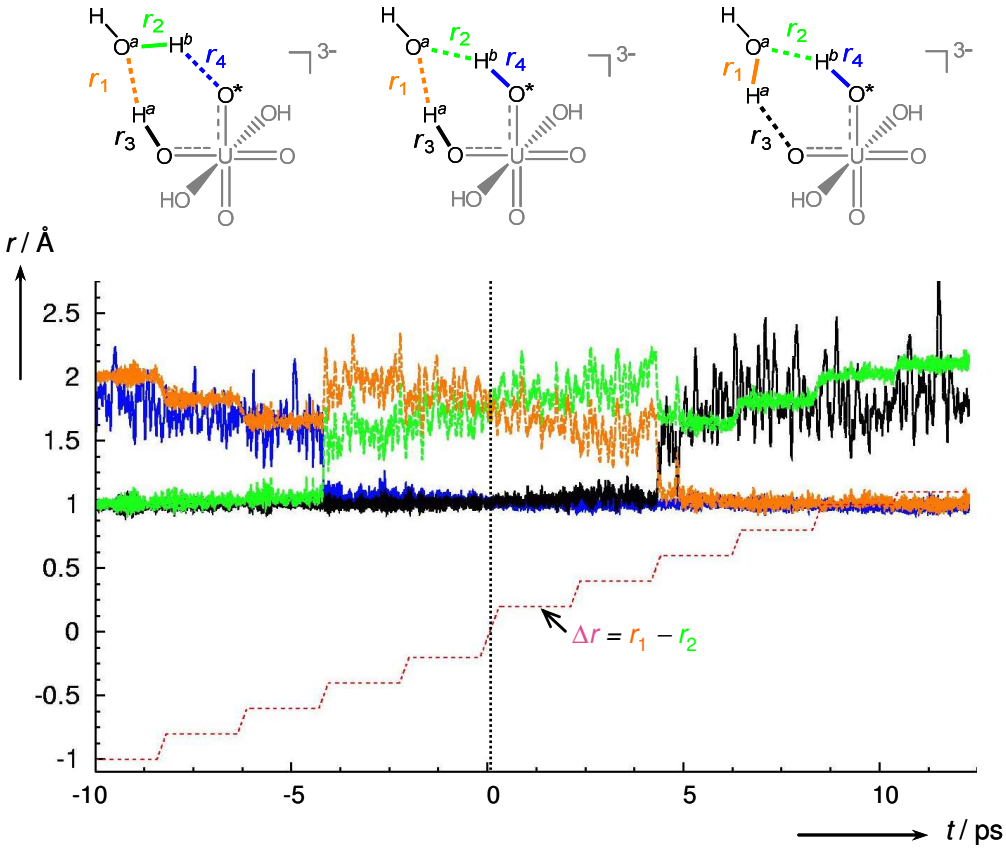

Figure 2: Evolution of selected OH distances along the continuous constrained paths starting from $\Delta r = 0$ (vertical dashed line). The "reverse" path ($\Delta r < 0$) is plotted in negative time.

In Figure 2, these two proton jumps at $t \approx -4$ and +5 ps seem to mark discontinuities on the path, indicating that the chosen reaction coordinate may not be ideal. As the mean constraint force changes appreciably before and after the jump (see Table S1 in the Supporting Information, SI), two additional points at $\Delta r = \pm 0.5$ Å were constructed, starting from the corresponding, preceding ones at $\Delta r = \pm 0.4$ Å. Since the two jumps had occurred either within the growth period between $\Delta r = -0.4$ Å to -0.6 Å, or shortly after that between $\Delta r = 0.4$ Å to 0.6 Å, it was hoped that in those points at half way, reversible proton jumps could be detected. Instead, in the simulation at $\Delta r = -0.5$ Å the proton jump occurred right away, whereas in that at $\Delta r = +0.5$ Å, it did not occur at all. As a consequence, the absolute values of the resulting mean constraint forces at the two points differed significantly (see Table S1). In principle, both simulations would have to be extended until so many reversible jumps have occurred that both constraint

forces have averaged to the same, absolute value. In practice, this may require exceedingly long simulation times.

The following, more pragmatic approach was therefore adopted: The $\langle f \rangle$ values on Δr = +0.2 Å, 0.4 Å, 0.6 Å, 0.8 Å, 1.0 Å and 1.1 Å were mapped onto those of the corresponding negative Δr points and both sets were pairwise averaged (for better numerical precision, see Table S1 for the actual data). Two integrals were then evaluated for ΔA by integration from Δr = −1.1 Å to zero (according eq 1), one using the original $\langle f \rangle$ value from Δr = −0.5 Å, and one using the mapped value from Δr = 0.5 Å. The resulting, highest points at Δr = −0.4 Å amounted to $\Delta A^{\ddagger}$ = 6.4 kcal/mol and 4.4 kcal/mol, respectively, and were used as error bars for the mean value taken at that point, $\Delta A^{\ddagger}$ = 5.4 ±1.0 kcal/mol. This procedure resulted in the free-energy half-profile shown in Figure 3.

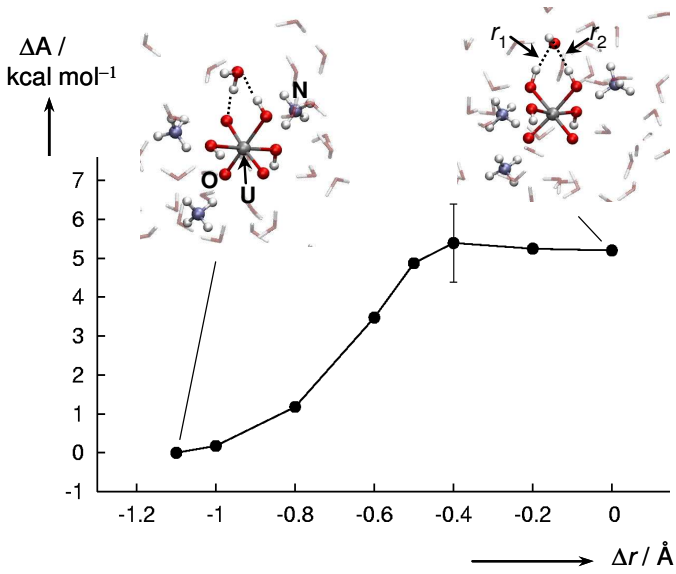

Figure 3. CPMD/BLYP simulated free-energy profile from **4**·H_2O (left) to **5** (or rather, **2**·OH^-, right) at 320 K, using the difference in the designated O···H distances r_1 and r_2 as reaction coordinate. For the estimated error bar at the highest point see text.

With the chosen reaction coordinate, **5** appears to be centered at a very flat part of the free-energy surface between Δr = −0.4 Å and +0.4 Å. Starting from **4**, this region is reached at $\Delta A^{\ddagger}$ = 5.4 ±1.0 kcal/mol, in excellent agreement with the static PBE-ZORA/COSMO data, $\Delta G^{\ddagger}$ = 5.7 kcal/mol.[9] The apparent feasibility of the proton shuttle mechanism predicted at that level is thus fully supported by our simulations in a more realistic, dynamic environment.

3.3 Energetics of cis-Uranyl Hydroxide

The structure of transient **5** is of particular interest. The initial constrained MD with $\Delta r = 0$ was started with similar O-H^a, O*-H^b, and O^a-H^a/O^a-H^b distances, all around 1.4 Å (labeling see Scheme 1, corresponding to r_1 - r_4 in Figure 2). Very rapidly, within 0.2 ps, both protons H^a and H^b moved to the metal-bound oxo atoms, affording hydroxo ligands with normal OH distances of 1.03(4) Å (average over the last 1.5 ps, standard deviation in parentheses). The O^a-H^a and O^a-H^b distances, constrained to be equal, attained much larger values, 1.79(16) Å on average. The structure of **5** thus resembles that of a *cis*-$[UO_2(OH)_4]^{2-}$ core chelating an OH^- ion via two H-bonds (i.e. **2**·OH^-). Only at Δr around ca. ±0.5 Å does the distance between O^a and H^a or H^b close to that of a normal OH bond. This leads to the surprising conclusion that even on the UO_3 pathway a *cis*-uranyl species is involved, i.e. that both "non-classical" ions **2** and **4** could play a vital role in an oxygen exchange process. When the simulation of **5** (or rather, **2**·OH^-) at $\Delta r = 0$ is continued without this constraint, that structure remains stable for ca. 0.4 ps, before a proton jumps over from **2** to OH^-, affording **4**. During that time, the (U)O-H bond that is about to break can complete more than 20 O-H stretching vibrations, suggesting that in the actual aqueous solution, **5** is a short-lived intermediate rather than a transition state.[42]

Chart 1

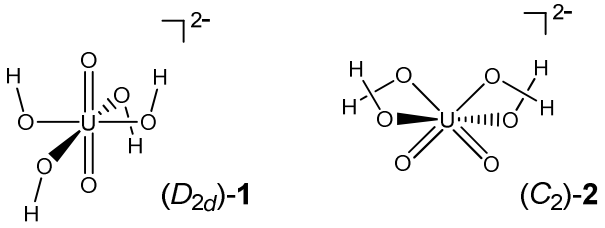

(D_{2d})-**1** (C_2)-**2**

According to our refined scrambling mechanism (see discussion below), the activation barrier essentially arises from the intrinsic energetic difference between the regular *trans*-uranyl species **1** and its *cis*-isomer **2** (in form of the OH^- complex **5**). In order to study the dependence of this relative stability of the two species on the level of theory, we evaluated the energy difference between two representative isomers, (D_{2d})-**1** and (C_2)-**2** (Chart 1), using a variety of DFT- and wavefunction-based methods. The results are summarized in Table 1 (for additional data including PCM values, see Table S2 in the SI).

The purpose of this exercise is not to provide a definitive value for this energy difference (a much more involved study including conformational analysis and basis-set convergence tests would be necessary for this), but rather to assess the performance of DFT, and BLYP in particular, in relation to the "gold standard" of quantum chemistry, CCSD(T). As can be seen from the data in Table 1, the source of the geometries is not overly important (compare the first three BLYP entries). B3LYP reproduces the CCSD(T) benchmark, 19.4 kcal/mol, to within 1 kcal/mol,[43] whereas BLYP (and PBE, another typical

GGA) underestimates it by ca. 6 kcal/mol. Noticeably higher numbers are obtained with the M06 series of functionals from the Truhlar group. Perturbation theory clearly cannot be applied to this problem, as evidenced by the strong oscillations in the MP*n* series. It should be noted, however, that CCSD(T) may also be close to the limits of its applicability. Estimated from the CCSD amplitudes, the so-called T_1-diagnostic[44] affords values of 0.023 and 0.025 for (D_{2d})-**1** and (C_2)-**2**, respectively, i.e. slightly higher than the accepted value of 0.02, above which the wavefunction is indicated to lose its single-reference character. Thus, more sophisticated multi-reference methods may be needed for a final answer.

Table 1: Potential energy of (C_2)-**2** relative to (D_{2d})-**1** (see Chart 1), obtained from single-point energy calculations with various methods.

Level[a]	E_{rel} [kcal/mol]
CP-opt/BLYP[b]	15.2
BLYP[c]	13.4
BLYP[d]	13.0
BLYP	13.0
PBE	13.7
B3LYP	18.5
M06-L	17.0
M06	22.7
M06-2X	24.0
HF	35.3
MP2	11.7
MP3	35.6
MP4sdq	−3.2
CCSD	26.0
CCSD(T)	19.4

[a]SDD(g)/aug-cc-pVTZ basis and B3LYP/SDD/6-311+G(d,p) geometries, unless otherwise noted; PCM denotes polarizable continuum modelling bulk water. [b]Optimized using the CPMD program and the same setup as in the CPMD simulations (except for an otherwise empty box). [c]CP-opt gas-phase geometries employed. [d]B3LYP/SDD/6-311+G(d,p) gas-phase geometries.

4. Discussion

The two consecutive steps simulated with CPMD, deprotonation and proton shuttle, can be combined into a continuous path affording the yl-exchange in **1**. We now compare the resulting mechanism, depicted in Scheme 2, to that proposed by Shamov and Schreckenbach on the basis of their static PBE-ZORA/COSMO calculations.[9]

Firstly, the possible involvement of the intriguing T-shaped tris(oxo) species **4** is fully corroborated by our simulations. Our computed barrier for formation of **4** via deprotonation of **1**, $\Delta A^{\ddagger}$ = 6.2 kcal/mol (Figure 1; 8.6 kcal/mol including the ion-pairing estimate), is even smaller than that reported by Shamov and Schreckenbach via OH^- addition to **1**, $\Delta G^{\ddagger}$ = 21.3 kcal/mol ($\Delta H^{\ddagger}$ = 12.5 kcal/mol).[9] Because no coordinative bonds are formed or broken during simple deprotonation, this single-step process circumvents **3** and provides a rather facile pathway for the formation of the key intermediate **4**. We cannot exclude that some fraction of the latter could be formed via **3**, but this is not relevant for the remaining discussion, and we have only included the direct, least-motion path in Scheme 2.

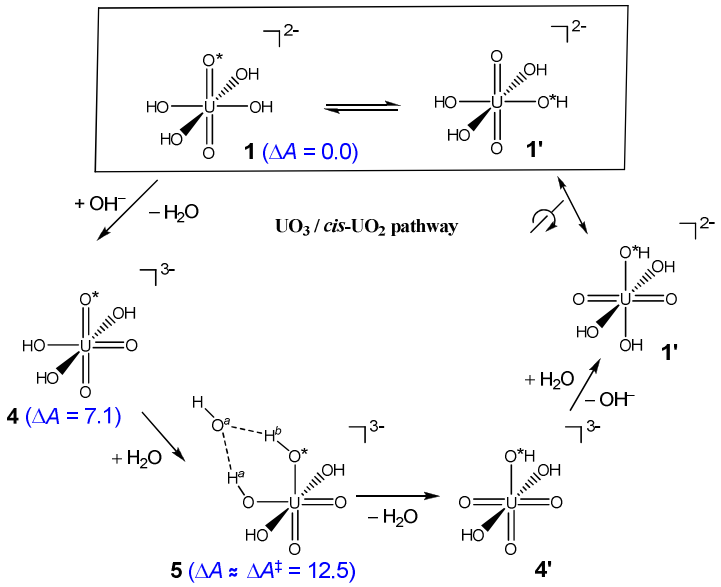

Scheme 2. CPMD-derived mechanism for oxygen exchange in aqueous uranyl hydroxide (in parentheses in blue: ΔA values in kcal/mol).

Secondly, the solvent-assisted proton-shuttle mechanism in **4** is fully corroborated in the dynamic aqueous environment, proceeding via a short-lived intermediate (or transition state) **5**, which can be described as a complex between *cis*-uranyl species **2** and OH^-. Starting from **1**, the area around **5** corresponds to the highest point on our overall scrambling path. Combining the estimated ΔA for formation of **4** discussed in section 3.1 above with $\Delta A^{\ddagger}$ from Figure 3 affords a total scrambling barrier of

$\Delta A^{\ddagger}$ = 12.5±1.3 kcal/mol (see SI for estimating the total error).[45] Despite different rate-limiting steps in the present and in Shamov and Schreckenbach's mechanism (proton shuttle in **4** and OH^- addition to **1**, respectively), both agree qualitatively that the yl-exchange should be a thermally feasible process. In terms of free energies, we find a somewhat lower overall barrier, $\Delta A^{\ddagger}$ = 12.5 kcal/mol via proton shuttling, as compared to Shamov and Schreckenbach's $\Delta G^{\ddagger}$ = 21.3 kcal/mol via OH^- addition.[9] The main conclusion at this point is that for whatever reason (which may well involve fortuitous error cancellation) there is no evidence for a dramatic failure of PCM-type solvation models in static DFT computations for the title reaction.

While our $\Delta A^{\ddagger}$ value is in good apparent accord with the barrier reported by Clark et al., $\Delta G^{\ddagger}$ = 15.2 kcal/mol,[4] it is in clear contrast to Szabo and Grenthe's initial failure to observe yl-exchange in **1**.[6] From the undiminished intensity of the ^{17}O NMR uranyl sinal of enriched **1**, a large barrier on the order of ca. 30 kcal/mol would be estimated.[46] Clark et al.'s barrier was obtained indirectly from line-shape analysis of the uranyl ^{17}O NMR signal, whereas Szabo and Grenthe followed the time evolution of this signal, which seemed to be a much more direct assessment and free of ambiguities (note, however, the recent reappraisal of these findings[7] discussed below).

Returning to our simulations, we now discuss methodological issues that could compromise their accuracy. The most important of these is the sensitivity of the results toward the particular exchange-correlation functional.[47] In those cases where precise experimental data on ligand binding energies or displacement barriers are available, our CPMD/BLYP approach has reproduced the experimental numbers to within ca. ±2.5 kcal/mol.[15-17] In all of these cases, however, the linear uranyl unit had stayed intact, thus facilitating error cancellation. For the thermochemistry of reactions involving the uranyl unit, hybrid functionals such as B3LYP tend to perform better than pure GGAs (such as BLYP).[13] Unfortunately, CPMD is impracticable with hybrids. Since our CPMD/BLYP-derived overall barrier is related to the relative stability of *cis*- and *trans*-uranyl hydroxide, however, to a first approximation we can use the static energetic data from Table 1 as incremental corrections to the barrier. Adding the difference between the CP-opt and the B3LYP value from Table 1, 3.3 kcal/mol, to the CPMD-derived scrambling barrier ($\Delta A^{\ddagger}$ = 12.5±1.3 kcal/mol) affords an estimate of $\Delta A^{\ddagger}_{B3LYP} \approx$ 16 kcal/mol. Using the CCSD(T) value from Table 1, the same procedure results in an estimate of $\Delta A^{\ddagger}_{CCSD(T)} \approx$ 17 kcal/mol. Using gas-phase ab initio or DFT results to correct solution-phase DFT/BLYP data should not be critical in this particular case, as bulk solvation effects on the relative energy of (D_{2d})-**1** and (C_2)-**2** are indicated to be very small (compare, e.g., B3LYP/SDD/6-311+G(d,p) and B3LYP/SDD/6-311+G(d,p)/PCM values

in Table S2), and the differential effect of specific electrostatic and H-bonding interactions with counterions and solvent should be captured reasonably well at the DFT/BLYP level.

Recently, Truhlar's M06 hybrid functional (which had been parametrized against test sets containing transition-metal compounds)[36] has been advocated as competitive with high-level ab initio methods for the water-exchange barrier and redox potentials of actinide complexes.[48] The increment method discussed above yields an estimate of $\Delta A^{\ddagger}_{M06} \approx 20$ kcal/mol. A slightly higher value, by about 1 kcal/mol is obtained with the M06-2X variant (designed and parametrized for main-group chemistry), and a much smaller one with the nonhybrid version M06-L (see data in Table 1). Thus, all DFT and ab initio methods applied so far agree that the actual scrambling barrier should not exceed 20 kcal/mol, with the CCSD(T)-based value of 16.7 kcal/mol as, arguably, the best estimate.[49]

At this point, spurred by the accumulated theoretical evidence that we had shared with them, Szabo and Grenthe decided to reinvestigate their original NMR evidence, which was crucial for their initial conclusion that there should be no exchange. As detailed in their new communication,[7] monitoring just the ^{17}O NMR signal of the uranyl moiety was incomplete. Looking at the intensity of the water signal now has revealed that by the time the first spectrum was recorded, scrambling had already occurred. The observation of a time-independent signal intensity is thus not indicative of very slow exchange, but to the contrary, of a very fast one. In fact, using a state-of-the-art NMR technique based on ^{17}O magnetization transfer, Szabo and Grenthe have now essentially reproduced Clark et al.'s activation parameters,[7] reconciling the conflicting interpretations of the experimental data and bringing theory and experiment back in concert. They also have shown now that the rate of exchange increases with the hydroxide concentration, consistent with the involvement of **3** and/or an outer-sphere complex between **1** and OH^- in the scrambling process.

Interestingly, at high uranyl concentrations Szabo and Grenthe have found evidence for a second-order rate law with respect to that uranyl concentration,[7] implying that a binuclear mechanism is operative under these conditions, similar to what has been inferred for the yl-exchange in cationic uranyl hydrate in acidic solution.[6] As no binuclear complexes can be formed under the periodic boundary conditions of our simulations, our results can be regarded as representative for dilute uranyl solutions of high ionic strength (a situation difficult to model in static computations). The possible competition of a binuclear mechanism is an intriguing topic for further computational studies.

5. Conclusion

Using state-of-the-art quantum-chemical methods that explicitly include effects of scalar relativity, solvation, counterions, and dynamics, we have studied a pathway for axial and equatorial "yl-exchange" in aqueous uranyl hydroxide, $[UO_2(OH)_4]^{2-}$, which refines a mechanism proposed recently on the basis of static DFT computations with a simpler solvation model. Not only can we corroborate $[UO_3(OH)_3]^{3-}$ with a T-shaped UO_3 core as viable intermediate, we also find that a transient species containing the *cis*-$[UO_2(OH)_4]^{2-}$ moiety can be involved in this process.

The computed overall barrier for this path is $\Delta A^{\ddagger} \approx 17$ kcal/mol at the CPMD/BLYP level with a CCSD(T)-derived correction. This value is in very good accord with the scrambling barriers reported in two independent experimental studies. In one of the latter, a revision of the initial interpretation of the data was necessary to achieve this mutual accord. This reconciliation of two, at first conflicting experimental studies underscores the potential usefulness of first-principles MD simulations in uranyl chemistry. For the title system, these simulations provide evidence that both a T-shaped tris(oxo) as well as a *cis*-uranyl hydroxide complex can be involved in a rapid exchange process. Both ions have intriguing structures and are unprecedented in the aqueous phase. Uranyl chemistry may be even richer and more diverse than it is already.

Acknowledgments

This work was supported by EaStChem via the EaStChem Research Computing facility and a local Opteron PC cluster maintained by Dr. H. Früchtl. G.S. acknowledges support from NSERC. We thank D. Clark, I. Grenthe, and Z. Szabo for stimulating and fruitful discussions, and the latter two for sharing their new experimental results prior to publication.

Supporting Information available on the WWW under http://www.pubs.acs.org or from the authors (additional computational details, graphical, and tabular material, full citations of refs. 37,38, as well as B3LYP geometries of D_{2d}-**1** and C_2-**2**).

References

(1) Denning, R. G. *J. Phys. Chem. A* **2007**, *111*, 4125-4143.

(2) Arnold, P. L.; Love, J. B.; Patel, D. *Coord. Chem. Rev*. **2009**, *253*, 1973-1978.

(3) Arnold, P. L.; Patel, D.; Blake, A. J.; Wilson, C.; Love, J. B. *J. Am. Chem. Soc.* **2006**, *128*, 9610-9611.

(4) Clark, D. L.; Conradson, S. D.; Donohoe, R. J.; Keogh, D. W.; Morris, D. E;. Palmer, P. D.; Rogers, R. D.; Tait, C. D. *Inorg. Chem*. **1999**, 38, 1456-1466.

(5) Wahlgren, U.; Moll, H.; Grenthe, I.; Schimmelpfennig, B.; Maron, L.; Vallet, V.; Gropen, O. *J. Phys. Chem. A* **1999**, *103*, 8257-8264.

(6) Szabo, Z.; Grenthe, I. *Inorg. Chem*. **2007**, *46*, 9372-9378.

(7) Szabo, Z.; Grenthe, I., submitted to *Inorg. Chem*.

(8) Schreckenbach, G.; Hay, P. J.; Martin, R. L. *Inorg. Chem*. **1998**, *37*, 4442-4451.

(9) Shamov, G. A.; Schreckenbach, G. *J. Am. Chem. Soc*. **2008**, *130*, 13735-13744.

(10) Green, D. W.; Reedy, G. T.; Gabelnick, S. D. *J. Chem. Phys*. **1980**, *73*, 4207-4216.

(11) Fore some selected reviews see: (a) Denning, R. G. *J. Phys. Chem. A* **2007**, *111*, 4125-4143. (b) Vallet, V.; Macak, P.; Wahlgren, U.; Grenthe, I. *Theor. Chem. Acc*. **2006**, *115*, 145-160. (c) Szabó, Z.; Toraishi, T.; Vallet, V.; Grenthe, I. *Coord. Chem. Rev.* **2006**, *250*, 784-815. (d) Kaltsoyannis, N.; Hay, P. J.; Li, J.; Blaudeau, J. P.; Bursten, B. E., in: *The Chemistry of the Actinide and Transactinide Elements*, 3rd ed.; Morss, L. R., Edelstein, N. M., Fuger, J., Katz, J. J., Eds.; Springer: Dordrecht, The Netherlands, 2006; Vol. 3, pp 1893-2012.

(12) Schreckenbach, G.; Shamov, G. A. *Acc. Chem. Res*. **2010**, *43*, 19-29.

(13) see e.g. Shamov, G. A.; Schreckenbach, G.; Vo, T. N. *Chem. Eur. J*. **2007**, *13*, 4932-4947.

(14) (a) Hay, P. J.; Martin, R. L.; Schreckenbach, G. *J. Phys. Chem. A* **2000**, *104*, 6259-6270; (b) Tsushima, S.; Yang, T.; Suzuki, A. *Chem. Phys. Lett*. **2001**, *334*, 365-373.

(15) (a) Bühl, M.; Sieffert, N.; Wipff, G. *Chem. Phys. Lett*. **2009**, *467*, 287-293. (b) Bühl, M.; Sieffert, N.; Golubnychiy, V.; Wipff, G. *J. Phys. Chem. A* **2008**, *112*, 2428-2436.

(16) Bühl, M.; Kabrede, H. *ChemPhysChem* **2006**, *7*, 2290-2293.

(17) (a) Barrier for water exchange: Bühl, M.; Kabrede, H. *ChemPhysChem* **2006**, *7*, 2290-2293; (b) binding energy of nitrate: Bühl, M.; Golubnychiy, V. *Inorg. Chem*. **2007**, *46*, 8129-8131.

(18) Car, R.; Parrinello, M. *Phys. Rev. Lett*. **1985**, *55*, 2471-2474.

(19) (a) Becke, A. D. *Phys. Rev. A* **1988**, *38*, 3098-3100. (b) Lee, C.; Yang, W.; Parr, R. G. *Phys. Rev. B* **1988**, *37*, 785-789.

(20) Troullier, N.; Martins, J. L. *Phys. Rev. B* **1991**, *43*, 1993-2006.

(21) Kleinman, L.; Bylander, D. M. *Phys. Rev. Lett.* **1982**, *48*, 1425-1428.

(22) Bühl, M.; Diss, R.; Wipff, G. *J. Am. Chem. Soc*. **2005**, *127*, 13506-13507.

(23) Marx, D.; Hutter, J.; Parrinello, M. *Chem. Phys. Lett*. **1995**, *241*, 457-462.

(24) Bühl, M.; Grigoleit, S.; Kabrede, H.; Mauschick, F. T. *Chem. Eur. J*. **2006**, *12*, 477-488.

(25) The initial CPMD/BLYP simulations in the Parrinello group have afforded good descriptions of liquid water, see for instance: (a) Sprik, M.; Hutter, J.; Parrinello, M. *J. Chem. Phys*. **1996**, *105*, 1142-1152, although potential shortcomings of this functional are now better appreciated, see: (b) VandeVondele, J.; Mohamed, F.; Krack, M.; Hutter, J.; Sprik, M.; Parrinello, M. *J. Chem. Phys.* **2005**, *122*, 014515 and references cited therein.

(26) Sprik, M.; Ciccotti, G. *J. Chem. Phys*. **1998**, *109*, 7737-7744, and references cited therein.

(27) Bühl, M.; Schreckenbach, G.; Sieffert, N.; Wipff, G. *Inorg. Chem*. **2009**, *48*, 9977-9979.

(28) CPMD Version 3.13.1, Copyright IBM Corp. 1990-2008, Copyright MPI für Festkörperforschung Stuttgart 1997 - 2001.

(29) Becke, A. D. *J. Chem. Phys.* **1993**, *98*, 5648-5642.

(30) Küchle, W.; Dolg, M.; Stoll, H.; Preuss, H. *J. Chem. Phys*. **1994**, *100*, 7535.

(31) (a) Krishnan, R.; Binkley, J. S.; Seeger, R.; Pople, J. A. *J. Chem. Phys*. **1980**, *72*, 650-654; (b) Clark, T.; Chandrasekhar, J.; Spitznagel, G. W.; Schleyer, P. v. R. *J. Comput. Chem.* **1983**, *4*, 294-301.

(32) as implemented in Gaussian 03: (a) Barone, V.; Cossi, M.; Tomasi, J. *J. Comput. Chem.* **1998**, *19*, 404-417; (b) Cossi, M.; Scalmani, G.; Rega, N.; Barone, V. *J. Chem. Phys*. **2002**, *117*, 43-54. (c) Cossi, M.; Crescenzi, O. *J. Chem. Phys.* **2003**, *19*, 8863-8872.

(33) (a) Dunning, Jr.; T. H. *J. Chem. Phys*. **1989**, *90*, 1007-1023; (b) Kendall, R. A.; Dunning, Jr.; T. H.; Harrison, R. A. *J. Chem. Phys*. **1992**, *96*, 6769-6806.

(34) Perdew, J. P.; Burke, K.; Ernzerhof, M., *Phys. Rev. Lett.* **1996**, *77*, 3865-3868.

(35) Zhao, Y.; Truhlar, D. G. *J. Chem. Phys*. **2006**, *125*, 194101

(36) Zhao, Y.; Truhlar, D. G. *Theor. Chem. Acct*. **2008**, *120*, 215-241

(37) (a) Frisch, M. J.; Pople, J. A.; et al., Gaussian 03, Revision E.01, Gaussian, Inc., Pittsburgh PA, 2003; (b) Frisch, M. J. et al., Gaussian 09, Revision A.02, Gaussian, Inc., Wallingford CT, 2009.

(38) Werner, H.-J.; Knowles, P. J.; et al., MOLPRO 2006.1, Cardiff, 2006.

(39) The choice of NH_4^+ as model counterion is motivated by its small size and the lack of a rigid hydration sphere, which (unlike e.g., simple alkali-metal ions) can result in less hindered tumbling and noticeable diffusive mobility on the picosecond timescale, thereby facilitating equilibration in the MD simulations. In order to prevent deprotonation (which cannot happen with the ions used experimentally), rigid NH_4^+ ions have been used.

(40) At this point, no assumption for the formation mechanism of **4** is implied; changes in free energies of start and end points of a thermodynamic integration are, at least in principle, independent of the path between them.

(41) See for instance: Morel, F. M. M.; Hering, J. G. *Principles and Applications of Aquatic Chemistry*, Wiley, New York, 1993, p. 399, where a simple expression for electrostatic interactions between ions in a dielectric continuum was used for this estimate ($\log K \doteq -1.74$).

(42) The actual proton-shuttling transition states transpiring from Figures 2 and 3 would correspond to slightly asymmetric versions of **5** with $\Delta r \approx \pm 0.4$ Å; however, in view of the uncertainty of the free energies and the flatness of the corresponding energy surface, a precise location of the true transition state is difficult.

(43) This result is in line with previous findings for "difficult reactions" of uranium oxo fluorides (i.e. those involving the uranyl moiety), where B3LYP performs very well, cf. reference 13.

(44) Lee, T. J.; Taylor, P. R. *Int. J. Quantum Chem. Symp*. **1989**, *23*, 199-207.

(45) This uncertainty refers to the numerical precision of the PTI technique. The absolute uncertainty due to the accuracy of the underlying quantum-chemical methodology (density functional, pseudo-potential, basis set) is, arguably, still higher, and is at least ±2.5 kcal/mol, judged from the errors in computed kinetic and thermodynamic parameters relative to experiment (see references 15-17).

(46) In Figure S1(a) in the SI of reference 6, the ^{17}O NMR signal of the yl-ogygen atoms in **1** shows essentially undiminished intensity even after 110 days. Assuming a half-life of at least ten times as long, an upper limit for the rate constant of ca. 10^{-8} s^{-1} can be estimated, yielding a lower limit for the barrier from the simple Eyring equation, $\Delta G^{\ddagger} > 28$ kcal/mol.

(47) Convergence with respect to basis-set size (i.e. energy cutoff) is a potential concern, too. While with our pseudopotentials the total energies are not very well converged with an 80Ry cutoff, relative energies usually are. The same holds for the mean forces in the constraint MD simulations: in one test case, the absolute value of a mean constraint force decreased by ca. 6% on going from 80Ry to 100Ry cutoff (see Table S1), which would serve to slightly reduce the final scrambling barrier.

(48) Austin, J. P.; Burton, N. A.; Hillier, I. A.; Sundarajan, M.; Vincent, M. A. *Phys. Chem. Chem. Phys*. **2009**, *11*, 1143-1145.

(49) Note that D rather than H was employed in the CPMD simulations and that tunneling or zero-point effects have been neglected, which would serve to decrease the effective barrier.

Table of Contents

According to CPMD simulations, a viable pathway for the "yl-exchange" in a uranyl hydroxide complex proceeds via transient species containing a T-shaped UO3 or a cis-uranyl moiety, both highly unusual in aqueous uranium chemistry.